Biochimica et Biophysica Acta, 1145 (1993) 149–156

BBAMEM 75860

The location of amantadine hydrochloride and free base within phospholipid multilayers: a neutron and X-ray diffraction study

K.C. Duff [a], A.J. Cudmore [a] and J.P. Bradshaw [a,b]

[a] *Department of Biochemistry, University of Edinburgh, Edinburgh (UK) and* [b] *Department of Preclinical Veterinary Sciences, University of Edinburgh, Edinburgh (UK)*

(Received 6 May 1992)
(Revised manuscript received 19 October 1992)

Key words: Amantadine free base; Amantadine hydrochloride; Phospholipid multilayer; X-ray diffraction; NMR, ^{2}H-

Concomitant neutron and X-ray studies were undertaken in order to locate accurately the anti-influenza and Parkinson's disease drug amantadine in multilayers of 1,2-dioleoyl-*sn*-glycero-3-phosphocholine. The X-ray data were phased using the swelling series method and the neutron data were phased using D_2O/H_2O exchange and a variation of the isomorphous replacement technique. The sets of data complement each other and reveal two populations of amantadine within the bilayer. One site is close to the bilayer surface, the other is much deeper. The majority of the amantadine occupies the surface site. The relative occupancy, but not the position, of the two locations appears to be dependent upon the initial protonation state of the drug. No evidence of bilayer perturbation was observed with either the protonated or the deprotonated forms of amantadine.

Introduction

Amantadine (1-aminoadamantane hydrochloride) is licensed for the prophylaxis of influenza A infection and for treatment of both influenza and Parkinson's disease [1,2]. In the case of influenza, the efficacy of amantadine is postulated to involve interruption of viral-host cell membrane fusion and/or interference in haemagglutinin maturation [3,4]. The mechanism of action of amantadine in Parkinson's disease is probably related to its ability to increase presynaptic synthesis and release of dopamine. This effect is potentiated by the drug inhibiting dopamine reuptake [5]. These therapeutic processes are thought to include the involvement of the hydrophobic, lipophilic properties of the molecule [6].

Amantadine studies undertaken so far have been wide-ranging, including its effect on influenza infection and, more recently, its specific molecular effect on the viral protein which is implicated in this drug-induced prophylaxis, namely M2 [7]. A recent study has examined the role of amantadine in the stabilisation of clathrin-coated membrane vesicles, similar to those formed upon initial viral penetration by influenza, Semliki Forest and vesicular stomatitus virus [6]. However, other authors have reported that, although tromantadine (an amantadine derivative: *N*-1-adamantyl-*N*-[2-(dimethylamino)ethoxy]acetamide hydrochloride) appears to stabilise phospholipid bilayers, amantadine itself slightly lowers the temperature of the bilayer to hexagonal phase transition. Also, NMR studies have shown that amantadine is perturbing to the organisation and motional properties of phospholipids in the bilayer phase [8]. These results indicate an amantadine-mediated increase in disorder. It can therefore be seen that a certain degree of ambiguity exists in the available data.

As a prerequisite of further mechanistic studies of amantadine, we have undertaken a series of experiments to investigate the location of the drug within bilayers of 1,2-dioleoyl-*sn*-glycero-3-phosphocholine (DOPC). To reduce possible ambiguity in the results a single lipid species was used, DOPC being the most physiologically representative. We have also examined any differences between amantadine hydrochloride (HCl) and amantadine in its free base form (FB).

This report describes the use of a specific deuterium labelling technique to locate amantadine in synthetic multilayer membranes using neutron diffraction. These

Correspondence to: J.P. Bradshaw, Department of Biochemistry, University of Edinburgh, Hugh Robson Building, George Square, Edinburgh, EH8 9XK, UK.

Abbreviations: amantadine FB, 1-amino adamantane free base; amantadine HCl, 1-amino adamantane hydrochloride; DOPC, 1,2-dioleoyl-*sn*-glycero-3-phosphocholine; DOPE, 1,2-dioleoyl-*sn*-glycero-3-phosphoethanolamine; NMR, nuclear magnetic resonance spectroscopy; rh, relative humidity.

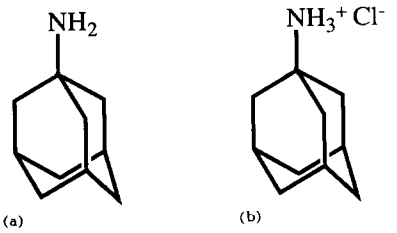

Fig. 1. The two forms of 1-aminoadamantane used in this study: (a) amantadine free base, (b) amantadine hydrochloride.

results are both quantitatively and qualitatively supported by a concomitant X-ray diffraction study using unlabelled amantadine.

Materials and Methods

1,2-Dioleoyl-*sn*-glycero-3-phosphocholine (DOPC) was purchased from Sigma (Fancy Road, Poole, UK) and confirmed to be a single species by thin-layer chromatography. Amantadine was obtained from the same source in both free base and hydrochloride forms (Fig. 1). Deuterated amantadine FB was obtained from Dr. M.R. Alecio of the Shell Research Centre (Sittingbourne, Kent, UK).

X-ray diffraction

Oriented phospholipid bilayer stacks were prepared as follows. Samples comprising 5 mg of DOPC with or without 5% (mol) amantadine were dissolved in methanol and applied to a curved glass support of approx. 1 cm^2 area. The solvent was allowed to evaporate before the slide was dried in vacuo for 2 h. Subsequently, the samples were hydrated for at least 2 h at 20°C and 100% humidity. Once fully hydrated, the samples were transferred to the sample cell of the X-ray camera.

For at least 1 h before and subsequently throughout the diffraction experiment, the samples were held in a purpose built environmental cell which allowed the temperature and humidity of the sample to be controlled. Temperature control was achieved by circulating water from a thermostat bath through tubes in the brass walls of the cell; all samples were run at 20°C at which DOPC adopts the L_α-phase. The humidity, and therefore the bilayer spacing, was controlled by passing air through containers of saturated salt solutions and then through the sample cell. Saturated solutions of $ZnSO_4$ (90% rh), KCl (81% rh), NaCl (74% rh) and NaBr (57% rh) were used in addition to distilled water (98% rh).

In the camera used to produce the diffraction patterns, 0.3 mm collimated, Nickel filtered copper K_α radiation of 1.54 Å from a Marconi-Elliot GX-13 rotating anode X-ray generator was scattered by the sample onto a pack of four 130 × 180 mm Agfa-Gevaert Osray X-ray films positioned 175 mm from the sample. The diffracted beam path was evacuated to reduce background noise from air-scattered radiation. To record the complete range of intensities without exceeding the films' dynamic range, each sample was exposed twice, typically for 20 h followed by a separate 4 min exposure. The developed films were scanned on a Joyce Loebl Chromoscan 3 microdensitometer.

Neutron diffraction

Sample preparation was essentially the same as described for the X-ray experiments, with the exception that each sample was 20 mg in weight and prepared on a quartz microscope slide. D_2O/H_2O exchange was achieved by dehydrating the samples in vacuo before re-equilibration over the new solvent.

Neutron diffraction data were collected using the D16 instrument at the Institut Max von Laue - Paul Langevin, Grenoble, France. After rehydration the quartz slide bearing its oriented multi-bilayer phospholipid sample was placed in the temperature controlled cell of the instrument along with water baths containing either D_2O or H_2O where it was allowed a further period of equilibration of 0.5–1 h. During this period the equilibration process was monitored by recording the angular position of the third or fourth order of lamellar diffraction which increased as the multilayers dehydrated and decreased as they took up water from the atmosphere. Each sample was judged to have achieved equilibrium when there was no further shift in the position of the Bragg peaks and the calculated lamellar repeat distance was that predicted for the experimental conditions by previous X-ray work. Any sample which did not fulfil both of these criteria was discarded. Each recorded diffraction pattern consisted of at least eight well defined orders. The mosaic spread of each sample was determined using the D16 software.

X-ray data analysis

The background scattering level was estimated by measuring the optical density of each X-ray film in the region immediately adjacent to a diffraction peak and interpolating across its base. Any peaks in which the dynamic range of the film had been exceeded were ignored. After integration of the diffracted intensities the films were scaled together using overlapping peaks and averaged to obtain the final set of intensities. A Lorentz factor was applied to take into account the spreading of the intensity in reciprocal space and the sampling of the peaks by the Ewald sphere. The diffraction peaks were discrete and well defined and were restricted to the meridional region of the film. In such situations, the Lorentz factor takes the form of $\sin(2\theta_h)$, where θ is the Bragg angle and h the order of diffraction. A further correction was applied for absorption of the incident and diffracted beams by the

lipid film [9]. Data sets of Bragg intensities (I_h) were scaled to each other using the expression:

$$\Sigma I_h = D/D_{\min}$$

where D is the Bragg spacing (bilayer repeat distance) and $D_{\min}$ represents the minimum Bragg spacing of a series run at different humidities.

D for each sample was determined using the Bragg equation. The instrument offset angle for each sample was calculated by iterative least squares regression of this equation over all observed orders of diffraction.

Neutron data analysis

Once the diffracted intensities had been corrected for detector response and background then integrated, the following corrections were applied:

(1) Acceptance angle. The projection of the quartz slide along the normal to the neutron beam is dependent upon its relative angle to the beam. If the slide presents a very low angle (θ) to the incident beam, it only samples a small fraction of the total neutron beam width and, therefore, flux. This means that the diffraction peaks recorded for the lower orders will be correspondingly weaker than if the slide were able to sample the whole width of the neutron beam. As long as the neutron beam is wider than the maximum projected width of the sample slide and the neutron flux constant across the width of the beam, the angular correction factor, takes the form:

$$C_{\mathrm{Ang}(h)} = 1/\sin\,\theta_h$$

(2) Lorentz factor. For the geometry used in this study, the appropriate correction factor is:

$$C_{\mathrm{Lor}(h)} = \sin(2\theta_h)$$

(3) Absorption. When the angle of diffraction is low, the incident and diffracted beam have a significant path length within the sample and thus will be subject to a greater degree of absorption than when the angle is high and the corresponding path lengths low. Moreover, the degree of absorption will also be affected by the H_2O/D_2O composition of the sample. The appropriate correction for absorption by the lipid film, was applied:

$$C_{\mathrm{Abs}(h)} = 1/(\sin\,\theta/2ut)(1 - \exp[-2ut/\sin\,\theta])$$

where $u = (6.04\text{–}0.75d)$, d being the mole fraction of D_2O [10]. The mass of lipid on each slide, the area over which it was spread and the unit cell size, as determined by diffraction, were used to calculate a value of 30 μm for t, the thickness of the lipid film.

(4) Sampling by the detector. As a result of lattice disorder in the sample, the diffraction peaks may be so wide that the whole of each diffraction peak is not recorded by the detector, and a correction must be applied to the data to account for this. In this study the mosaic spread of each sample was small enough to ensure that each diffraction peak was regular in shape and contained wholly within the central part of the detector so no correction was applied in this case.

The final neutron structure factor amplitudes were therefore calculated as:

$$F_h^2 = I_h \cdot C_{\mathrm{Ang}(h)} \cdot C_{\mathrm{Lor}(h)} \cdot C_{\mathrm{Abs}(h)}$$

Phasing

Electron density or neutron scattering profiles may only be obtained upon solving the individual phases of the recorded amplitudes. In this study three different techniques were employed to phase the data sets: swelling series, D_2O/H_2O exchange and isomorphous replacement.

The X-ray structure factors were phased using a five point swelling series [11]. Our methodology comprised of selecting from the swelling series one working set of eight diffraction peaks and using this to compute a continuous transform [12] against which the fit of all the other observed sets were compared. The best fit minimised the difference between the calculated and the observed intensities for each of the possible 256 phase combinations. The selected working set alternated until all five had been used and sampled against. The resulting transform represented the best, integrated fit for all data over all possible phases. This process was carried out independently for the DOPC, DOPC/amantadine HCl and DOPC/amantadine FB swelling series.

Neutron data are routinely phased by carrying out experiments hydrated at various H_2O/D_2O ratios [9,10,13,14]. This method was used in the present study, with additional phasing information coming from a variation of the isomorphous derivative technique [15] in which use was made of the presence or absence of amantadine in the multilayers. Assigning phases to the neutron data proceeded by altering the sign of the individual structure factors until a result was achieved in which both the differences caused by replacing H_2O with D_2O and the DOPC/amantadine minus DOPC differences were consistent within each set of comparable data.

The two techniques, using X-rays and neutrons, emphasise different features within the bilayer structure, and further confirmation that the correct phases had been assigned was given by the fact that the two methods agreed and thereby showed the complementary nature of the techniques.

White and his co-workers [16] have produced an elegant method for scaling neutron data. This approach was used in the present study and basically involved using the size of the D_2O and the amantadine distributions to scale the different sets of data to each other. The results put the profiles on a 'relative absolute' scale in which they are scaled with respect to the unit cell contents, but not on an absolute per volume scale. The method is also readily applicable to X-ray data, although for this there is no equivalent of the D_2O peak therefore scaling is carried out on the size of the amantadine distribution alone.

Results

Fig. 2 is a representative X-ray diffraction pattern, in this instance obtained from DOPC with 5% (mol) amantadine FB at 90% rh. Fig. 3 shows the relationship between the relative humidity of the sample chamber and the bilayer repeat distance as observed by X-ray and neutron diffraction. Fig. 4 shows the swelling series data used to phase the X-ray diffraction patterns of pure DOPC (a), DOPC with 5% (mol) amantadine HCl (b) and DOPC with 5% (mol) amantadine FB (c). In each case the continuous transform calculated from 98% rh data is shown superimposed upon the observed diffraction amplitudes for 98, 90, 81, 74 and 57% rh. Table I gives the corrected, scaled neutron diffraction structure factors for all three samples at 0% and 100% D_2O. Fig. 5 shows reconstructed transbilayer profiles of DOPC alone (a, b) and difference profiles calculated by subtraction of structure factor data sets of corresponding *D*-repeat to define the distribution of amantadine HCl (c, d) and FB (e, f), respectively.

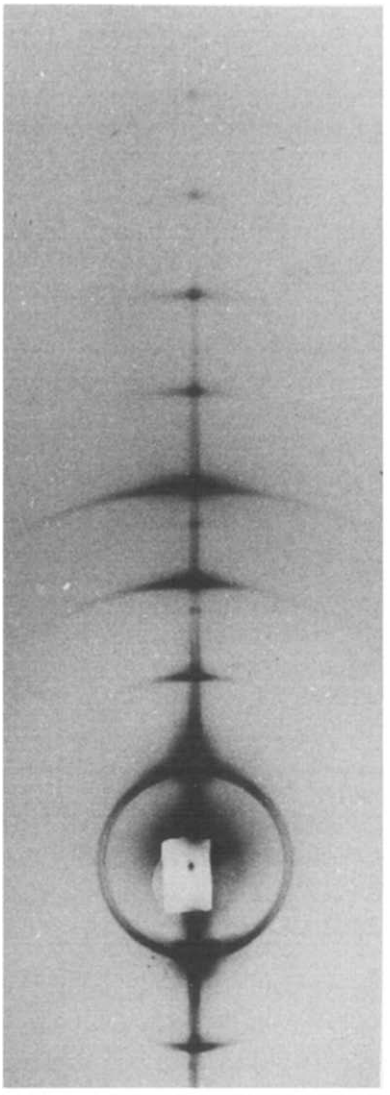

Fig. 2. X-ray diffraction pattern of lamellar arrays of DOPC with 5% (mol) amantadine FB at 90% relative humidity and 20°C.

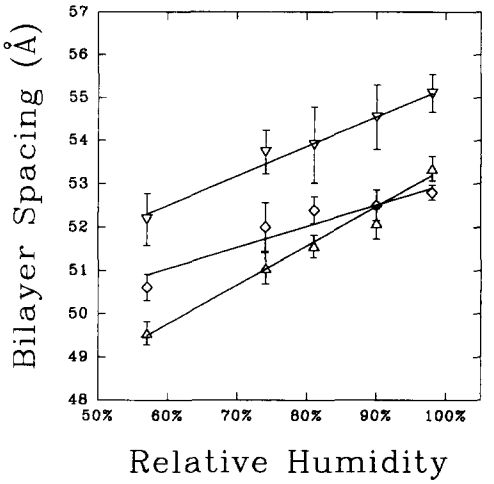

Fig. 3. The relationship between the relative humidity at 20°C of the sample and the observed bilayer spacing (in ångströms, Å). ▽, pure DOPC; △, amantadine hydrochloride; ◇, amantadine free base. The error bars represent the standard deviation for each point. Sample size varied from 3 to 9.

The mosaic spread of the DOPC bilayers ranged from 0.4° to 0.6°, these very low values being quite characteristic of unsaturated fatty acyl phospholipids. The mosaic spread was not significantly changed upon the addition of amantadine.

Discussion

DOPC

Fig. 5 displays both X-ray and neutron scattering density profiles across the phospholipid bilayer with the water component occupying the outer region of the graphs. With X-rays, the DOPC profile (a) agrees with previously published data [17,18] in that it displays the classic phospholipid leaflet form with a main peak representing the electron-dense region which encompases the phosphate groups and fatty acyl ester bonds. A secondary peak appears within the hydrophobic region which corresponds to the double-bond in the oleic

acid chains. It can be seen from (b) that less detail results from the neutron data. This is probably due to the lower contrast characteristic of neutron scattering (all diffraction experiments were sampled through eight orders so this phenomenon does not involve the X-ray data being collected to a higher resolution than the neutron).

The differences between the X-ray and neutron profiles are due to inherent atomic scattering differences across the unit cell. X-rays are more strongly scattered by the phosphate groups in the repeat motif whereas maximum neutron scattering corresponds to the fatty acyl ester bond positions [19]. Profile (b) clearly displays this scattering dichotomy with the neutron data peak appearing markedly closer to the hydrophobic interior of the bilayer than the X-ray result (a). The sharper X-ray profile displays a second highly defined peak in the fatty acyl chain region of the leaflet.

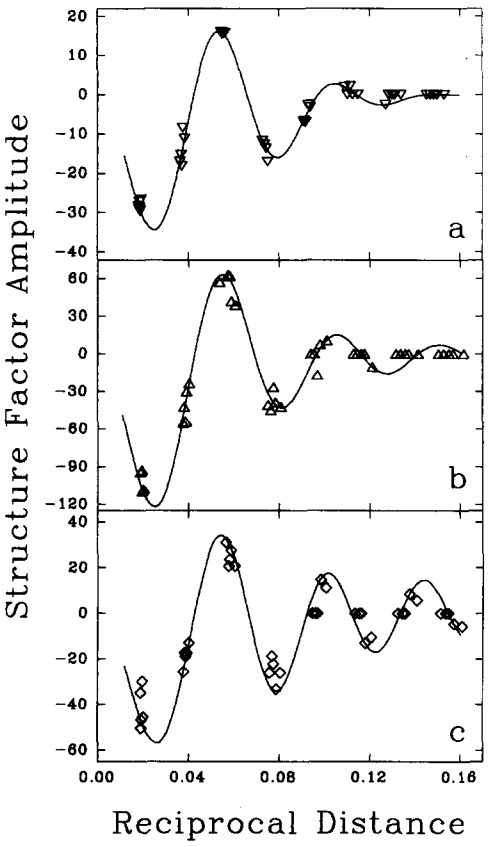

Fig. 4. Structure factors of lamellar arrays of bilayers of (a) pure DOPC, (b) DOPC with 5% (mol) amantadine HCl and (c) DOPC with 5% (mol) amantadine FB, plotted against corresponding reciprocals of Bragg spacings ($Å^{-1}$). The amplitudes of the structure factors are equal to the square roots of the Bragg intensities, their signs are those derived from the phasing procedure described in the text. The swelling series data sets were collected at 98, 90, 81, 74 and 57% relative humidity. The continuous transforms calculated from the 98% rh data is shown.

TABLE I

Relative absolute neutron structure factors of lamellar arrays of pure DOPC and DOPC with 5% (mol) amantadine HCl or FB at 98% rh and 20°C. The accuracy is estimated to be ± 0.15 units

Order	DOPC 20°C, 98%rh (D_2O)	DOPC+5 mol% amantadine HCl 20°C, 98%rh (D_2O)	DOPC+5 mol% D-amantadine FB 20°C, 98%rh (D_2O)
1	−89.31	−61.22	−96.41
2	25.56	10.02	18.80
3	−4.34	−1.68	−2.76
4	1.00	0.32	1.21
5	−2.84	−1.86	−2.97
6	0.77	0.06	0.57
7	−0.67	0.15	−0.16
8	0.00	−0.27	−0.15
Order	DOPC 20°C, 98%rh (H_2O)	DOPC+5 mol% amantadine HCl 20°C, 98%rh (H_2O)	DOPC+5 mol% D-amantadine FB 20°C, 98%rh (H_2O)
1	−6.47	−19.74	−13.55
2	−12.09	−8.66	−17.65
3	5.16	3.17	6.53
4	0.34	0.00	0.00
5	−1.44	−1.37	−1.98
6	0.33	−0.18	0.33
7	−0.30	0.26	0.00
8	0.00	−0.30	0.00

Amantadine HCl

Fig. 5. (c) to (f) are difference profiles which were calculated by subtracting the lipid component from the lipid + amantadine structure factors and therefore represent only the amantadine distribution across the bilayer. They are displayed in the same orientation as the pure DOPC but it can be seen that these profiles, both X-ray and neutron, are substantially different from the DOPC data. Amantadine, in both its hydrochloride and free base forms, appears to have been incorporated into the multilayer system.

The highest peak in the X-ray profile (c), representing the greatest distribution of amantadine HCl, lies between the phosphate and ester linkages. This surface location is also represented in the neutron (d) profile but its shape has changed with additional density encroaching into the water. It is proposed that the difference between the X-ray and neutron profiles is due to the relatively higher scattering length of nitrogen for neutrons compared to that for X-rays, which emphasises the amine group in the neutron profiles. These results therefore orientate amantadine HCl in the bilayer; the hydrophobic, cyclic region of the drug located between the phosphate and ester linkages of the phospholipids with the NH_3^+ group protruding into the water space.

This interpretation is supported by changes in the distribution of water between adjacent bilayers when amantadine HCl is added. Fig. 6 shows difference profiles representing the location of the deuterons of

heavy water, calculated by subtracting neutron scattering profiles of multi-bilayers containing H_2O from corresponding ones hydrated with D_2O. It can be seen that incorporation of amantadine HCl into the DOPC bilayers reduces the area under the water profiles, indicating that the drug is displacing some of the water from the system.

Both profiles (c) and (d) of Fig. 5 include additional features in the lipid tail region which may be caused by termination error. The resolution of the present study procludes unambiguous assignment of these features to the presence of amantadine deep within the bilayer, but it should be noted that evidence from the FB profiles (see below) indicates that full penetration of the bilayer by a proportion of the amantadine can occur. This is particularly noticeable in the neutron profiles and is either a product of the relatively high concentration of drug used saturating preferential surface sites, or it may represent amantadine which has reverted to the uncharged, FB form by deprotonation.

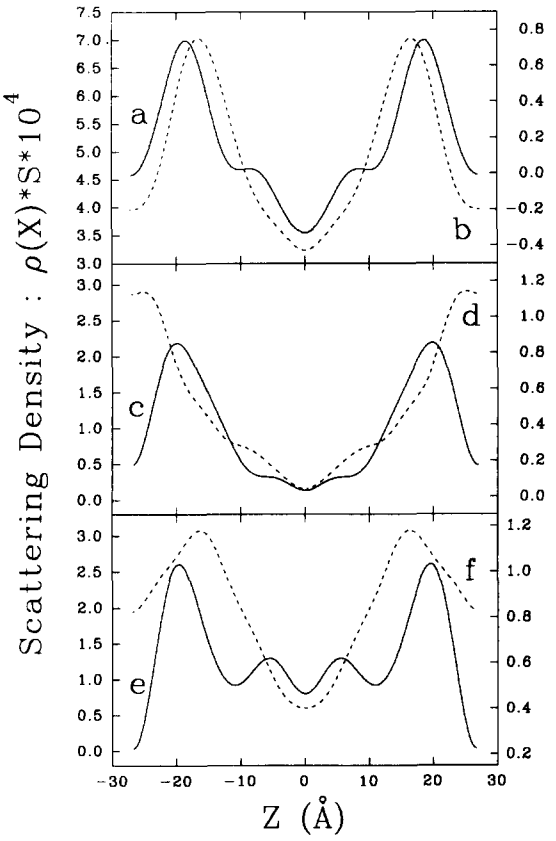

Fig. 5. Reconstructed trans-bilayer X-ray scattering profile of pure DOPC (a, left-hand scale) and neutron scattering profile of pure DOPC (b, right-hand scale) at 98% rh and 20°C. (d) and (f) are neutron scattering difference profiles of amantadine hydrochloride and amantadine free base, respectively. (c) and (e) are the corresponding X-ray scattering difference profiles. The difference profiles were calculated by subtracting structure factors of pure DOPC from those of DOPC with 5% (mol) amantadine, after correction for variations in bilayer repeat and placed on a relative absolute scale using the method of Weiner et al. [18]). The horizontal scale (Z) is distance, measured from the bilayer centre, in ångströms.

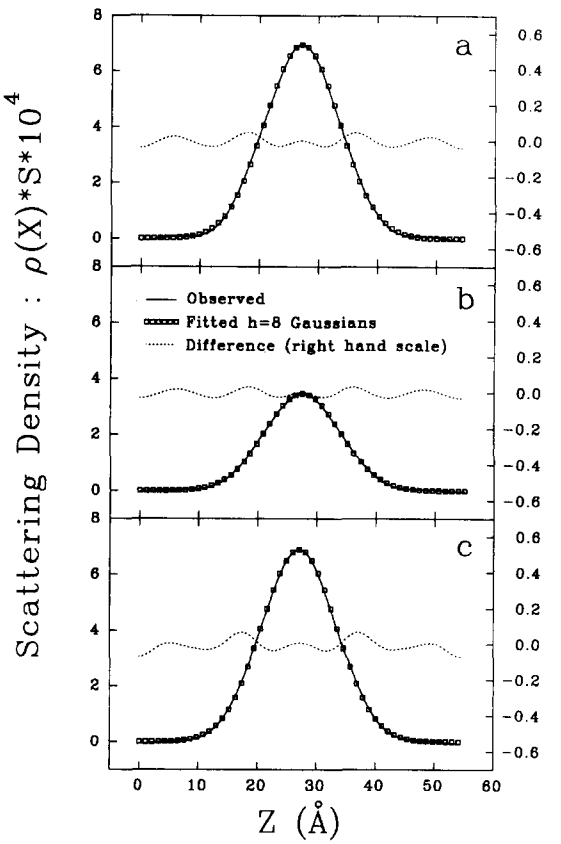

Fig. 6. Difference neutron density scattering profiles showing the distribution of water between bilayers of (a) pure DOPC, (b) DOPC with 5% (mol) amantadine HCl and (c) DOPC with 5% (mol) amantadine FB, all at 20°C. Also shown are Gaussian distributions fitted to the water profiles in reciprocal space over all eight observed orders of diffraction, using a development of the method of Wiener et al. [18]. Each curve consists of the sum of two Gaussians with the following parameters: (a) Z (distance from centre of bilayer) = $\pm 26.53 \pm 0.35$ Å, A_w (1/e halfwidth) = 8.82 ± 0.20 Å; (b) $Z = 26.04 \pm 0.55$ Å, $A_w = 8.75 \pm 0.25$ Å; (c) $Z = \pm 25.58 \pm 0.45$ Å, $A_w = 8.65 \pm 0.25$ Å. The difference between the observed and modelled water profiles may be taken as a crude approximation of error in the reconstructions. Each graph therefore also shows this difference, plotted on an enlarged scale, corresponding to that used in Fig. 5 (right-hand side).

Amantadine FB

At this resolution, both amantadine peaks are in the same position in the X-ray profile (e) as in the amantadine HCl result (c). Positionally, therefore, the data are identical. However, there is a difference in the proportional representation of amantadine across the bilayer with relatively more now appearing in the fatty acid tail region of the phospholipids. The neutron results (f) support these findings. Here the main scattering density at the surface location has moved slightly into the bilayer reflecting the fact that the amantadine FB is deuterated on the hydrophobic carbons only and that the NH_2 amine group is unlabelled and therefore scatters much less intensely compared to the labelled

mass; it can be observed as a shoulder on the water side of the main peak. This observation again orientates the amantadine with its NH_2 group at the lipid/water interface.

Profiles (e) and (f) clearly show that a proportion of amantadine has penetrated almost to the centre of the bilayer. Once again, the features in this region may represent some part of the amantadine structure, or may just be termination error. However, the height of the profiles above zero can only be explained in terms of a considerable mass of drug being present in this region. Consistent with this finding, the amount of water associated with the bilayers containing amantadine FB is much greater than that for bilayers containing amantadine HCl (Fig. 6) and almost equates with that present in the bilayers in the absence of either form of amantadine. Clearly a proportion of the drug has moved away from the water-penetrated surface of the bilayers to take up a deeper location in the bilayers. This evidence, taken together with the HCl results, leads us to propose that the interaction between amantadine and DOPC bilayers takes the form of an equilibrium between two possible regions. One of these is located at the water/bilayer interface, the other is less defined and broadly represents the fatty acid tail region. The balance of this equilibrium between the two sites appears to depend upon the starting protonation state of amantadine. However, this does not necessarily imply that the initial charge state of the amine is preserved throughout the experiment. This result compares with tetracaine where its interaction with phospholipids is also reported to be influenced by the charge state of the drug [20,21].

Amantadine–phospholipid interactions

If the optical parameters and the sample dimensions are kept constant throughout a series of diffraction experiments then the mosaic spread may be used as a measure of the macroscopic order of each sample; the smaller the mosaic spread, the less the degree of disorder of the bilayers [22,23]. The values obtained for stacked bilayers of pure DOPC in this study are in good agreement with previous observations [16,17]. The mosaic spread did not change upon the addition of 5 mol% amantadine, which indicates that the interaction between the drug and the bilayer did not disturb the macroscopic order of the system. There was no evidence of phase separation in the multilayers containing amantadine. Unfortunately, in the liquid phase, DOPC does not give discrete 4.5–4.8 Å reflections so we are unable to comment on the effect of amantadine on chain packing. We can, however, conclude that, under these experimental conditions, amantadine does not markedly perturb the bilayer system.

It has been reported that amantadine reduces the extent of dissociation of clathrin from coated vesicles [6] in a study which used relatively small amounts of the amine. The ability of amantadine and related compounds to stabilise or destabilise phospholipid bilayers has also been extensively investigated. Cheetam and Epand [8] concluded from NMR studies that amantadine perturbs the organisation and increases the fluidity of bilayers. Our present study, using a much lower drug/lipid molar ratio, does not indicate any such perturbation but it may be that this anomaly reflects the different drug concentrations used in such studies.

Another variable involves the lipid type used. The work reported here employed DOPC which has a large headgroup and two unsaturated chains giving the phospholipid a quasi-hourglass shape, creating an area of increased steric freedom in the neck region when the lipids are formed into a bilayer. The amantadine may be accomodated within such an area, fitting in between the phospholipid molecules. Our data, which indicate that the cyclic carbon component of amantadine orientates on the hydrophobic side of the phospholipid headgroup, support this model. This would suggest that the effects of amantadine upon bilayer structure and stability are likely to be complex and to be dependant upon intrinsic and environmental factors.

Fig. 2 shows that the bilayer repeat distance was reduced by up to 2.5 Å at low humidities. A similar effect is produced by the addition of 1,2-dioleoyl-*s*-glycero-3-phosphoethanolamine (DOPE) [17] to DOPC, where the smaller PE headgroup allows the choline moiety of DOPC to lie in a more perpendicular orientation and therefore closer to the plane of the bilayer surface (unpublished data). Amantadine may have a similar effect on DOPC. Unfortunately, the relatively low contrast between the PC headgroup and water makes it impossible to determine the headgroup conformation with the present data. However, this does mean that any drug-induced changes in headgroup conformation will not have an adverse effect on the profile subtractions. Future neutron work using specifically deuterated phospholipid headgroups may be able to resolve this question.

Our finding that uncharged, amantadine FB has the ability to penetrate more easily into the bilayer is supported by diffusion data performed on other similar compounds [24]. This phenomenon could be related to the zwitterionic nature of DOPC, the lipid chosen for our study. Further work will investigate the possible relationship between the lipid composition of the bilayer and the nature of its interaction with amantadine. For example, including a proportion of negatively-charged lipid may induce major changes [25] particularly with the charged amantadine HCl.

Acknowledgements

The deuterated amantadine was prepared by Dr. M.R. Alecio (Shell Research Centre, Sittingbourne,

UK) who also read and made helpful comments on the manuscript. Neutron data collection and initial reduction were performed on instrument DI6 at the Institut Max von Laue - Paul Langevin, Grenoble, France. The work was supported by both SERC and ILL grants.

References

1 Oxford, J.S. and Galbraith, A. (1980) Pharmacol. Therap. 11, 181–262.
2 Obeso, J.A. and Martinez-Lage, J.M. (1987) in: The Handbook of Parkinson's Disease (Koller, W.C., ed.), pp. 312–316, Marcel Dekker, New York.
3 Hay, A.J. (1989) in Concepts in Viral Pathogenesis, Vol. 3, pp. 561–567, Springer-Verlag, New York.
4 Sugrue, R.J., Bahadur, G., Zambon, M.C., Hall-Smith, M., Douglas, A.R. and Hay, A.J. (1990) EMBO. J. 9, 3469–3476.
5 Gilman, A.G., Rall, T.W., Nies, A.S. and Taylor, P. (1990) The Pharmaceutical Basis of Therapeutics, 8th Edn., pp. 472–473, Pergamon Press, New York.
6 Phonphok, Y. and Rosenthal, K.S. (1991) FEBS Lett. 281, 188–190.
7 Sugrue, R.J. and Hay, A.J. (1991) Virology 180, 617–624.
8 Cheetham, J.J. and Epand, R.M. (1987) Biosci. Rep. 7, 225–230.
9 Franks, N.P. and Lieb, W.R. (1979) J. Mol. Biol. 133, 469–500.
10 Worcester, D.L. and Franks, N.P. (1976) J. Mol. Biol. 100, 359–378.
11 Torbet, J. and Wilkins, M.H.F. (1976) J. Theor. Biol. 62, 447–458.
12 Lesslauer, W., Cain, J.J. and Blaisie, J.K. (1972) Proc. Natl. Acad. Sci. USA 69, 1499–1503.
13 Büldt, G., Gaily, H.U., Seelig, J. and Zaccai, G. (1979) J. Mol. Biol. 134, 673–691.
14 Jacobs, R.E. and White, S.H. (1989) Biochemistry 28, 3421–3437.
15 Büldt, G., Gaily, H.U., Seelig, A., Seelig, J. and Zaccai, G. (1978) Nature 271, 182–184.
16 Weiner, M.C., King, G.I. and White, S.H. (1991) Biophys. J. 60, 568–576.
17 Bradshaw, J.P., Edenborough, M., Sizer, P.J.H. and Watts, A. (1989) Biochim. Biophys.. Acta 987, 101–110.
18 Weiner, M.C. and White, S.H. (1991) Biochemistry 30, 6997–7008.
19 Franks, N.P. and Lieb, W.R. (1981) in Liposomes: From Physical Structure to Therapeutic Applications (Knight, ed.), pp. 243–272, Elsevier/North-Holland Press, Amsterdam.
20 Smith, I.C., Auger, M. and Jarrell, H.C. (1991) Ann. NY. Acad. Sci. 625, 668–684.
21 Shinooka, T., Shibata, A. and Terada, M. (1992) Biochim. Biophys. Acta. 1104, 261–268.
22 Schwartz, S., Cain, J.E., Dratz, E.A. and Blasie, J.K. (1975) Biophys. J. 15, 1201–1233.
23 Blaurock, A.E. and Nelander, J.C. (1976) J. Mol. Biol. 103, 421–431.
24 Miller, D.K. and Lenard, J. (1981) Proc. Natl. Acad. Sci. USA. 78, 3605–3609.
25 Kim, J., Mosior, M., Chung, L.A., Wu, H. and McLaughlin, S. (1991) Biophys. J. 60, 135–148.